Journal of Optics

PAPER

Shaping the on-axis intensity profile of generalized Bessel beams by iterative optimization methods

To cite this article: Runze Li *et al* 2018 *J. Opt.* **20** 085603

IOP Publishing Journal of Optics
J. Opt. **20** (2018) 085603 (10pp) https://doi.org/10.1088/2040-8986/aace46

Shaping the on-axis intensity profile of generalized Bessel beams by iterative optimization methods

Runze Li[1,2,3], Xianghua Yu[1], Tong Peng[1,2,3], Yanlong Yang[1], Baoli Yao[1], Chunmin Zhang[2] and Tong Ye[4,5]

[1] State Key Laboratory of Transient Optics and Photonics, Xi'an Institute of Optics and Precision Mechanics, Chinese Academy of Sciences, Xi'an 710119, People's Republic of China
[2] School of Science, Xi'an Jiaotong University, Xi'an 710049, People's Republic of China
[3] University of Chinese Academy of Sciences, Beijing 100049, People's Republic of China
[4] Department of Bioengineering, Clemson University, Clemson-MUSC Bioengineering Program, Charleston, SC 29425, United States of America

E-mail: yaobl@opt.ac.cn and ye7@clemson.edu

Received 15 April 2018, revised 11 June 2018
Accepted for publication 21 June 2018
Published 6 July 2018

Abstract
The Bessel beam belongs to a typical class of non-diffractive optical fields that are characterized by their invariant transverse profiles with the beam propagation. The extended and uniformed intensity profile in the axial direction is of great interest in many applications. However, ideal Bessel beams only rigorously exist in theory; the Bessel beams generated in the experiment are always quasi-Bessel beams with finite focal extensions and varying intensity profiles along the propagation axis. The ability to shape the on-axis intensity profile to meet specific needs is essential for many applications. Here, we demonstrate an iterative optimization based approach to engineer the on-axis intensity of Bessel beams through design and fine-tune processes. Starting with a standard axicon phase mask, the design process uses the computed on-axis beam profile as a feedback in the iterative optimization process, which searches for the optimal radial phase distribution that can generate a so-called generalized Bessel beam with the desired on-axis intensity profile. The fine-tune process repeats the optimization processing by using the adjusted target on-axis profile according to the measured one. Our proposed method has been demonstrated in engineering several quasi-Bessel beams with customized on-axis profiles. The high accuracy and high energy throughput merit its use in many applications. This method is also suitable to engineer higher-order Bessel beams by adding appropriate vortex phases into the designed phase mask.

Keywords: Bessel beam, on-axis intensity, iterative optimization, feedback

(Some figures may appear in colour only in the online journal)

1. Introduction

First introduced by Durnin [1, 2], the Bessel beam is a type of nondiffracting beams whose lateral beam profiles do not change with the propagation. For example, the zeroth-order Bessel beam has a lateral profile with a central lobe surrounded by an infinite number of concentric rings; this profile stays unchanged even when the beam propagates with an infinitely long distance. Given this unique property, the Bessel beam has been widely used in applications, such as optical trapping [3, 4], optical coherence tomography [5], fast volumetric imaging [6–10], and light sheet microscopy [11–14]. Multiple Bessel beams can interfere with each other to form more complicated beams such as the self-imaging bottle beam (SIBB), which has been of great interest in various applications [15–17]. Nonetheless, ideal Bessel beams

[5] Author to whom any correspondence should be addressed.

are only valid mathematically; the lab-generated Bessel beams are all quasi-Bessel beams existing in a limited space. In general, a quasi-Bessel beam is generated by passing a Gaussian beam through either a refractive or diffractive axicon; the refractive axicon is typically a conical lens fabricated by a special polishing process, while the diffractive axicon is implemented either by a phase control device such as a spatial light modulator (SLM) or a Fresnel lens based component [18]. One prominent feature of the quasi-Bessel beam is that its axial intensity profile varies with the beam propagation due to effects such as the limited beam diameter and imperfection in fabricating axicons [19, 20]. This feature hampers applications such as light sheet microscopy [11–14] and volumetric imaging [6–10], where the non-diffractive properties of the Bessel beam are expected. On the other hand, applications such as optical trapping [3, 4] require specific on-axis beam profiles to trap particles at certain locations. In both cases, the ability to modify the on-axis beam profile according to a certain distribution function is essential to an application. It has been demonstrated that the on-axis beam profile can be shaped to an arbitrary distribution, while the central lobe still maintains the invariant lateral profile within a limited region as in the case of the classical quasi-Bessel beam. However, as it does not necessarily maintain its side lobe profile invariant along the beam propagation, the newly generated beam falls into a category called the generalized Bessel beam, which exists both theoretically and experimentally [21–24].

Several approaches have been reported to engineer such generalized Bessel beams to obtain specific on-axis intensity distribution. The first approach is to design generalized axicons together with passive optical apodization components to flatten the on-axis intensity profile and to reduce the oscillation [21, 25, 26]. It was demonstrated that the on-axis intensity distribution could be determined by phase retardation function in radial direction [21]; the logarithmic axicon was then designed using the geometric optics principle. This approach was also used to design other types of generalized axicons to generate arbitrary on-axial intensity distribution. However, geometric optics cannot treat the diffraction effect; for example, the intensity oscillation caused by the edge blocking of a beam [19] cannot be evaluated during the design process. Anna Thaning [27] made an improvement by using stationary-phase method to design axicons with the inclusion of the oscillation property; the on-axis intensity oscillations were smoothed via the beam apodization. Generalized axicons were also designed for partially coherent source or oblique illumination for different applications [27]. However, the apodization needs an amplitude modulation and its capability for smooth the oscillations may be limited. Bi-Zhen Dong [28] presented an iterative method to design generalized axicon phases using Yang–Gu iterative algorithm. The on-axis intensity of Bessel beam was able to be programmed through controlling wavefront in multiple-output planes. However, the accuracy of on-axis intensity was limited by the number of output planes. The second approach, demonstrated by Zamboni-Rached [29, 30], superposes multiple Bessel beams with different spatial frequencies to enable the arbitrary control of the on-axis intensity. With this approach, Vieira and Dorrah [31–33] generated frozen waves in the experiment by superposing multiple modes of Bessel beams. However, the number of superposed Bessel beams was limited and thereby the freedom of arbitrary control of on-axis intensity was limited. The method utilized the concept of the spatial frequency of Bessel beams was introduced by Čižmár and Dholakia [34]. The on-axis intensity profile was customized by the spatial spectrum found by using a modified Gechberg–Saxton algorithm. Ouadghiri [35] has used this approach to shape the axial amplitude arbitrarily with a single phase only hologram. Though high quality axial intensity profiles were generated, the total energy throughputs were only around 10% [35] when the designed on-axis profile was realized experimentally. The low energy throughput reported in [34, 35] was mostly due to the holographic generation of the complex field; modulation of both phase and amplitude of the light field with the first diffraction order of the SLM led to poor utilization of energy.

In this report, we will first describe the mathematical relation between the phase retardation function of the axicon and its corresponding on-axis intensity distribution. Then we propose a new strategy to design a generalized Bessel beam according to a given on-axis intensity profile. During the design stage, a feedback optimization algorithm such as genetic algorithm (GA) [36–38] is used to search the optimal radial phase retardation that can generate Bessel beams with a desired on-axis intensity profile. The search starts with a standard axicon phase which is continuously modified by the algorithm. With each modified axicon phase, the on-axis intensity profile is computed and fed into a feedback tuning loop to approach the optimal design. During experimental implementation stage, a fine-tune process uses the experimentally acquired data to correct the design so that the consistency between the realized and the target on-axis intensity distribution is improved. Since this is a direct modulation method to generate Bessel beams, the energy throughput is significantly higher than the hologram based method, which renders its practical use in applications. This method can be also used to customize high-order Bessel beams with given longitude intensity distribution by superimposing appropriate vortex phases on the designed phase mask for zeroth-order Bessel beams. Diffraction at the cut off of the axicon is taken into consideration in the axicon design process, thus, more complex and smooth design results are gotten.

2. Methods

2.1. Formation of the on-axis field of generalized Bessel beams

With scalar diffraction theory and the paraxial approximations, the two-dimensional Fourier transform can be used to decompose a transverse field $U(x, y)$ into frequency components of plane waves [34]. Each frequency component is defined by the wave-vector $k = [k_x, k_y, k_z]$. If an SLM to generate Bessel beams is located at the zero of the z-axis (the propagation direction), the spatial frequency to form the transverse field at the position of the SLM can be expressed as:

$$S(k_x, k_y, z=0) = \iint_{-\infty}^{\infty} U_{SLM}(x, y, z=0)e^{-i(k_x x + k_y y)}dxdy, \tag{1}$$

where $U_{SLM} = A_0 e^{i\varphi}$ and is the complex transverse field right after the SLM when a plane wave with an amplitude $A_0(x, y)$ is incident upon the SLM applied with a phase mask $\varphi(x, y)$. For azimuthally symmetric field, (x, y) can be replaced by the transverse radial coordinate (r), where $r = \sqrt{x^2 + y^2}$. Similarly, (k_x, k_y) can be replaced by (k_r), where $k_r = \sqrt{k_x^2 + k_y^2}$. Accordingly, the Fourier transform is replaced by the Hankel transform and we rewrite equation (1) in the following form:

$$S(k_r, z=0) = \int_0^{\infty} U_{SLM}(r, z=0)J_0(k_r r)rdr, \tag{2}$$

where J_0 is the zeroth-order Bessel function of the first kind. The inverse transform of equation (2) is given by:

$$U_{SLM}(r, z=0) = \int_0^{\infty} S(k_r, z=0)J_0(k_r r)k_r dk_r, \tag{3}$$

The physical interpretation of equation (3) is that any azimuthal independent field, such as a Bessel beam, can be viewed as a composition of ideal zeroth-order Bessel beams with different k_r [34]. Each of these ideal Bessel beams propagates in the free space with a field $J_0(k_r r)e^{ik_z z}$, where z is the distance of propagation and k_z is the axial wave-vector component with $k_z = \sqrt{k^2 - k_r^2}$. The on-axis field is formed by the combination of those Bessel beams along the axis:

$$U_{axis}(r=0, z) = \int_0^{\infty} k_z S(\sqrt{k^2 - k_z^2}, z=0)e^{ik_z z}dk_z, \tag{4}$$

Equations (2) and (4) link the on-axis intensity distribution $|U_{axis}|^2$ with the modulation field U_{SLM}. If $|U_{axis}|^2$ is defined, U_{SLM} can be found by solving equations (2) and (4) numerically using algorithms such as iterative optimization methods. Essentially, it is the phase mask, $\varphi(r)$, that needs to be determined according to a user-defined target field.

2.2. Design the phase mask to generate a targeted Bessel beam with iterative optimization

A classical axicon is a phase control element whose phase retardation decreases linearly only in the radial direction. Modifying the phase retardation distribution radially would result in a generalized axicon phase that yields a generalized Bessel beam with a different on-axis profile, as discussed in 2.1 and illustrated in figure 1(a). The modification can be continuously made by an iterative optimization process while the on-axis intensity profile is calculated and compared with a targeted field. The iterative optimization process starts with a phase mask $\varphi(r)$, which transforms the incident plane wave $A_0(r)$ into a conic wave which forms a Bessel beam in the interference region. Then the calculated on-axis intensity is fed into the iterative optimization loop to search for optimum solutions for desired on-axis profiles. For simplicity of calculation, the incident light is a plane wave with uniform amplitude. We divide the radial phase retardation $\varphi(r)$ into N number of phase rings. Before optimization, these N variables hold the same phase values to form a classical axicon. In our case, the axicon phase mask was defined by an image of 600×600 pixels. Here, the iterative optimization is performed by GA, as shown in figure 1(b).

The genetic algorithm is chosen to optimize the N variables until a generalized axicon phase mask is found to form the desired intensity profile within a predefined error. GA is an iterative optimization algorithm inspired by species evolution and well suited for large-scale optimization problems [38]. Previous studies in the wavefront shaping [39] have shown that GA is an efficient and robust method that can optimize many phase segments in parallel and maintain a high stability in the noisy environment. The flowchart of GA is shown in figure 1(b). Here, independent N local retardation phases of the phase mask make up an individual. GA starts with an initial population of M phase masks. Each phase mask is the same original classical axicon with liner radial phase retardation as shown in figure 1(a). The difference between the computed on-axis intensity and the target profile is used as the cost function, which is calculated by summing all the absolute differences between the two intensity profiles at every axial position. Phase masks are ranked based on their cost functions with less difference ranked higher. Phase masks with higher ranks are more likely selected for evolution while the others are eliminated. Operations, known as elite, crossover, and mutation, are used to modify the selected phase masks to form a new generation for the next round in the iterative optimization. This process repeats until a predefined criterion is met. The termination criterion can be a single or multiple of the following conditions that are satisfied: reaching a predefined number of generations, reaching a specified running time, reaching a predefined value for the cost function, or when the reduction of the cost function is slowed down to a predefined speed. In our program, we terminated the GA process when the average relative change of the cost function was smaller than 0.1% over 50 generations of optimization.

The GA function in Global Optimization Toolbox of Matlab (MathWorks, USA) was used to perform all the optimization processes in this article. The parameters of GA were chosen in balance of the computing cost and the fineness of the searching process. A large population size ensures the diversity of individuals and guarantees the optimization efficiency of GA; however, this causes increased time cost of computing in each generation. The population size M was chosen to 40 as a good balance according to our experience. The elite count specifies the number of individuals that survive to the next generation and was set to 10 in our program. The elite count ensures the robust convergence of GA while too many elites will slow down the convergence rate of GA. The mutation makes small random changes of individuals in forming a new generation, i.e. the mutation represents the step size of searching the optimized phase. These changes should be kept small enough especially in the later stage of the optimization, otherwise the optimization may return with a bad or failed result. We chose a Gaussian mutation with a variance of 5 over the total depth of 256 gray levels, which were corresponding to the phase value from 0 to 2π. The

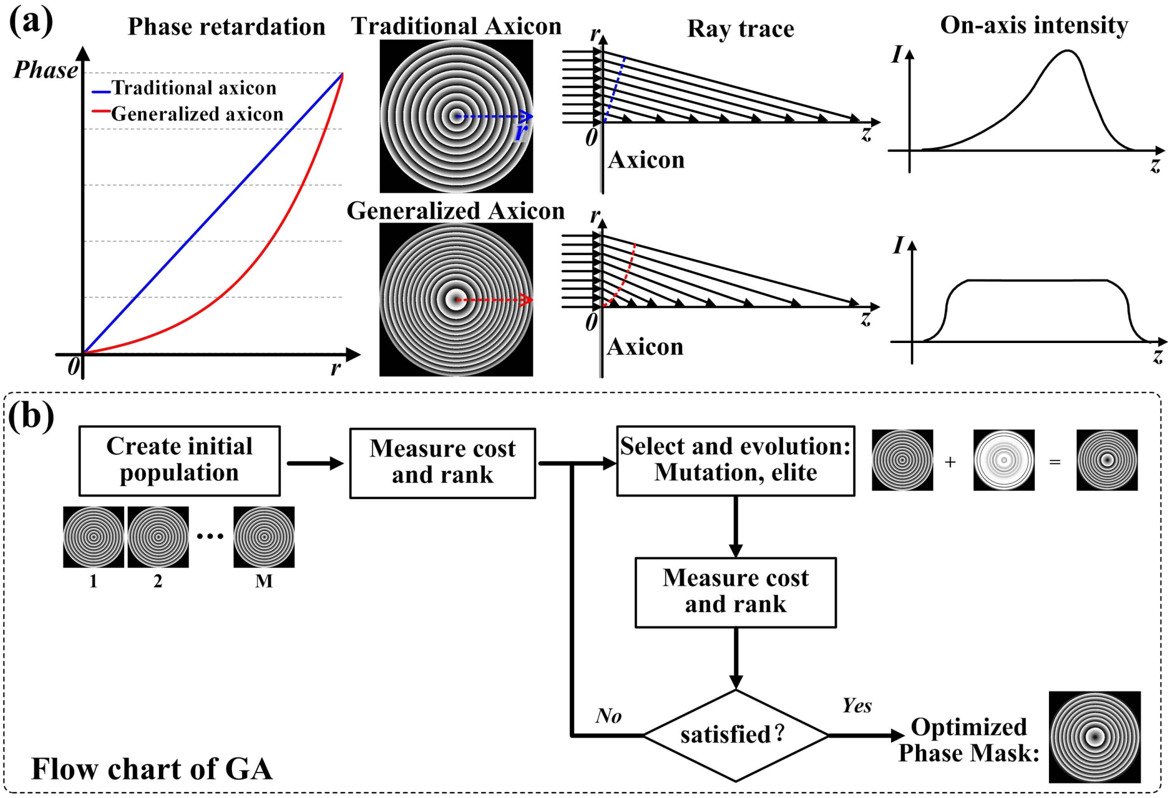

Figure 1. The principle of the iterative optimization process for shaping the on-axis intensity profile. (a) Effects of the phase retardation on the axial intensity. (b) Flowchart of the iterative optimization process implemented with the genetic algorithm.

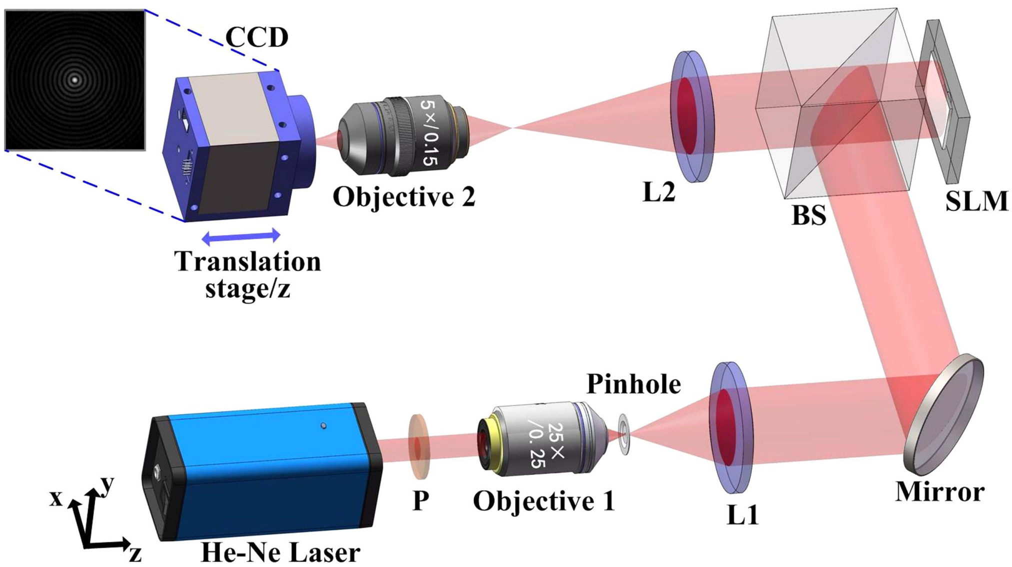

Figure 2. Experimental setup for measuring the three-dimensional intensity distribution of Bessel beams.

operation of crossover was disabled to preserve the precision in the phase mask design.

2.3. Experimental setup to implement the designed beam profile

Experimental set up for generation of Bessel beams and the beam profile measurement is shown in figure 2. A horizontal polarized 632.8 nm He–Ne laser beam is spatially filtered and expanded by a Galilean telescope which is composed of a 25× microscope objective, a 25 μm pinhole performs as a spatial filter, and a 150 mm lens (L1). The collimated beam is reflected by a beam splitter (BS) and is incident onto an SLM (PLUTO NIR-II, Holoeye Photonics AG, Germany). For the ease of detection, the Bessel beam generated by SLM is reduced 5 times by an imaging system constructed by a 200 mm lens (L2) and a 5× microscope objective (NA 0.15). Thus the engineered Bessel beam can be directly detected by

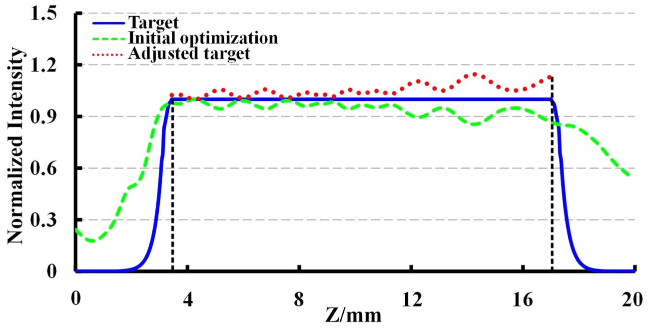

Figure 3. Illustration of the fine-tune step for generating flat top on-axis intensity distribution in experimental implementation.

a CCD camera (DCU224M, Thorlabs Inc., USA). To detect on-axis intensity distribution, the CCD camera is moved along the axis by a translation stage (MTS50/M-Z8, Thorlabs Inc., USA). The Bessel beam intensity was reconstructed by recording sequentially images along the propagation distance z. Because of the unideal performance of the SLM, there is a prominent zero-frequency which creates an additional background. A blazed grating is superimposed to the phase mask applied on the SLM for shifting the non-diffracted component off the imaging path.

2.4. Fine-tune in the experimental implementation

A small deviation was often found between the experimental and the simulation results. A trial-and-error approach was used to adjust the applied phase mask to reduce the deviation. Here we use the flat top on-axis Bessel beam as an example to illustrate the general concept of this fine-tune step. As shown in figure 3, the target on-axis intensity profile is in a flat top shape (in blue) while the experimental result (in green), which is generated by using the found phase mask from the GA optimization and the simulation, has oscillations and gradually drops its intensity along the beam propagation direction. To compensate the deviation, one approach we have been used is to fabricate a new target (in red) shown in figure 3 to feed the optimization loop. The new target is created by 'flipping' the experimental profile (in green) with respect to the original target (in blue) so that the weaker part is now stronger in the new target in hope of compensating the loss in the experiment. The new target is then entered into the GA optimization process going on to adjust the pre-founded phase mask and find the improved one. This procedure can be repeated multiple times to reach an acceptable improvement. As shown later in figure 5, after the fine-tuning process, the experimental result matches the 'flat top' target better than the green line does in figure 3. All the experimental results in this paper have undergone such a fine-tuning procedure. The total calculation time depends on the number of iterations. A complex target profile will take longer time due to more iterations needed in the optimization process. The amount of time spent on one design can have a large variation, spanning from tens of minutes to several hours. For time-sensitive applications, such as optical trapping and imaging, generalized axicon phases can be designed beforehand.

3. Results

We first wrote a simulation module to calculate the on-axis intensity of a generalized Bessel beam with a given phase mask according to the principle described in section 2.1. The simulation and experimental results of classical axicon phase mask are shown in figure 4. In the simulation, we calculated the transverse intensity fields every 0.08 mm to cover an axial distance of 40 mm. The data yield a 500-points on-axis intensity profile, which is plotted in figure 4(b). In the experiment, the on-axis intensity profile was obtained from 500 images taken at every 0.08 mm by the CCD camera. As seen in figure 4, the simulation and experimental results exhibit well-matched patterns of oscillations and peaks, although they both are obviously not uniform as an ideal Bessel beam is. This has demonstrated that the simulation module can successfully calculate the on-axis intensity profile according to a specific phase mask.

Then a GA based optimization program was implemented with the simulation module, which was used to design several phase masks that shaped quasi-Bessel beams according to the targeted on-axis intensity profiles, including linear increase, flat top, linear decrease, and sinusoidal fluctuation. The designed phase retardation, simulation outcomes, and experimental implementations are shown in figure 5. The experimental results present good resemblance to the targeted profiles. These results have demonstrated that the proposed iterative optimization method is effective to fabricate generalized Bessel beams whose on-axis intensity profiles need to be in desired shapes. These profiles can be useful in various applications. For example, the flat top Bessel beam can be used to increase the imaging field of view in light sheet microscopy; the linear increase can be used to compensate part of power loss when the Bessel beam propagates in absorption or scattering media [40]. The energy throughput of this method is much higher than the hologram based method, because the SLM performs like an axicon and used for phase only modulation. In our experiments, the reflectivity of SLM was about 75% and the first-order diffraction efficiency of the SLM was over 80% as specified by Holoeye [41]. Thus, the total efficiency of the Bessel beam generation by the SLM was estimated about 60%.

We further tested our method in engineering more complicated quasi-Bessel beams, including a high frequency, high contrast sinusoid, and a doublet-axicon-generated field. The high frequency and high contrast sinusoidal modulation may find its use in structured illumination microscopy, providing an illumination modulation in the axial direction. Formed by two axicons with different apex angles, a doublet axicon generates two co-propagating Bessel beams, which interfere with each other to form a so-called SIBB. The SIBB was used as optical tractor beams in the optical trapping application [4]. In both cases, the amplitude of the modulation varies with the beam propagation, which may affect their usefulness in applications. Using our proposed method, we have demonstrated that the amplitude of the modulation can be made uniform. The results are shown in figures 6(a) and (b), respectively.

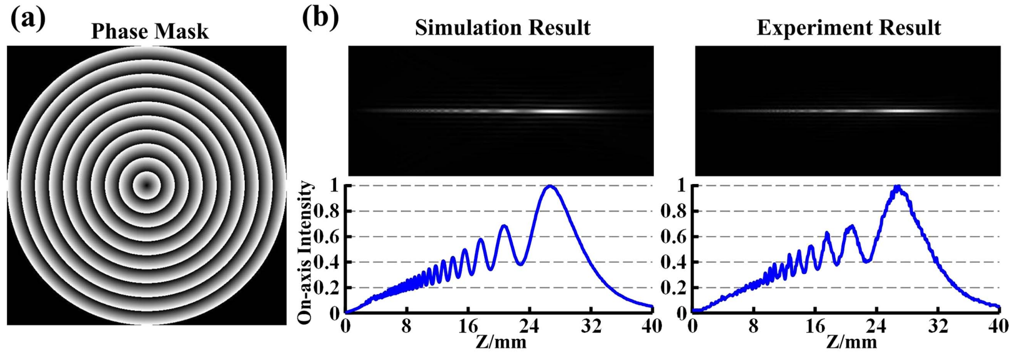

Figure 4. Simulation and experimental results of the on-axis intensity distribution of a classical axicon phase without optimization. (a) Phase mask; (b) the corresponding on-axis intensity of (a).

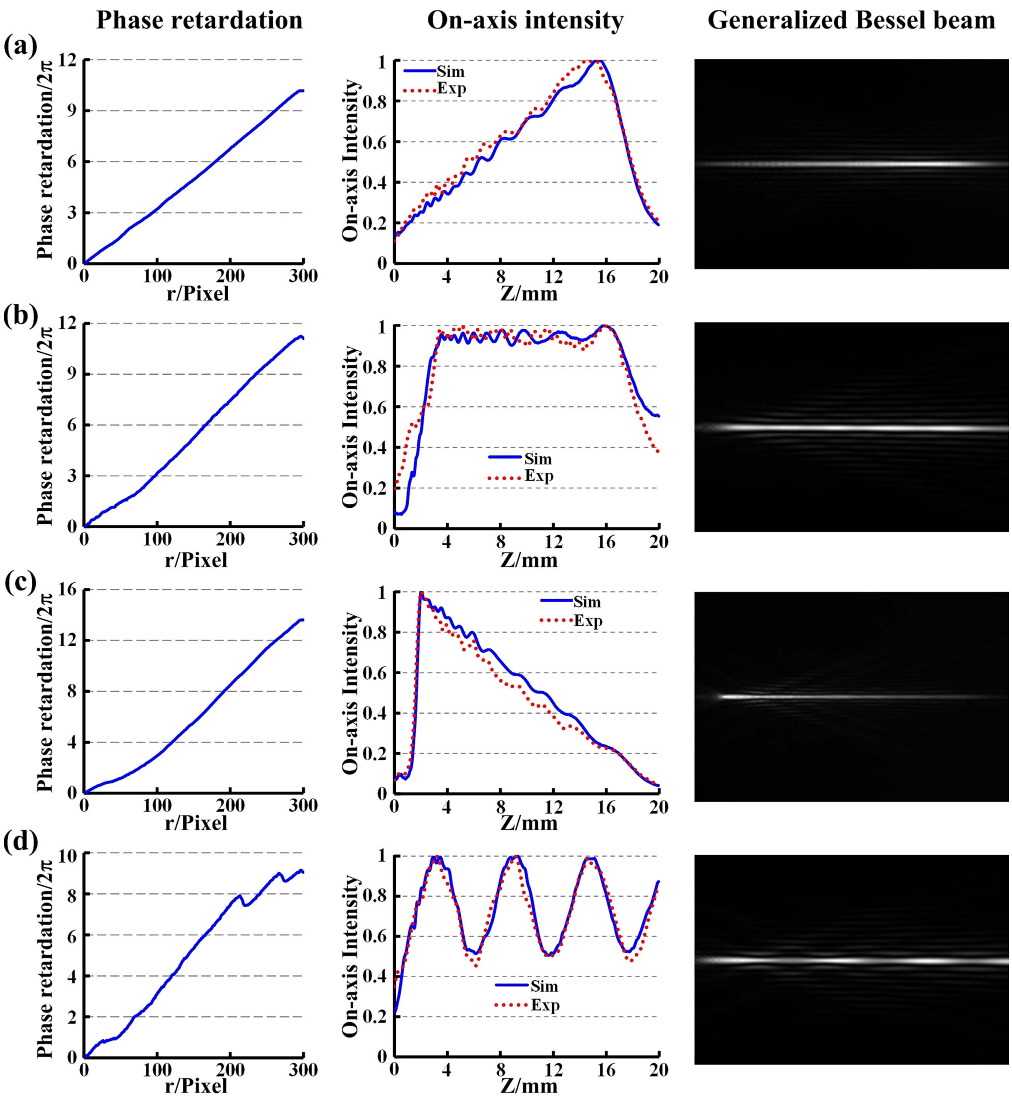

Figure 5. Simulation and experimental results of the designed phase masks and their corresponding on-axis intensity distributions. Left column: the designed phase retardation. Center column: the corresponding on-axis intensity of (a) line increase, (b) flat top, (c) line decrease and (d) sinusoidal distribution of simulation (Sim) and experiment (Exp) results. Right columns: the corresponding generalized Bessel beams detected in experiment.

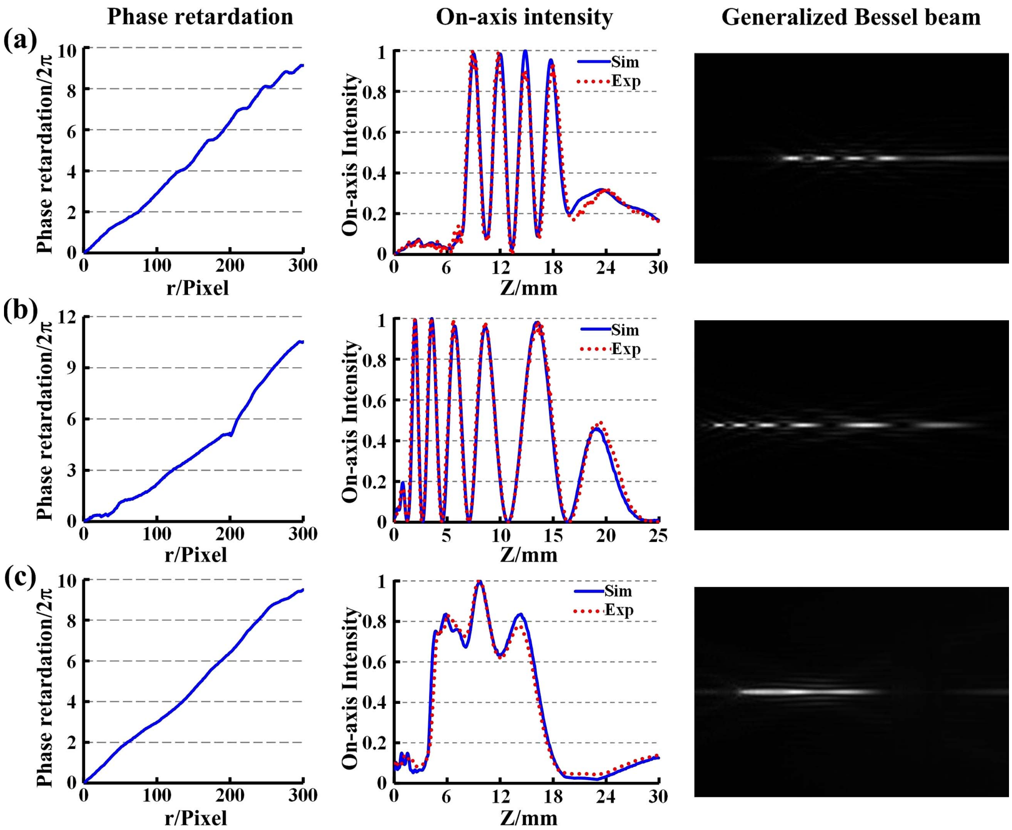

Figure 6. Simulation and experiment results of the designed phase masks and their corresponding on-axis intensity distributions. Left column: the designed phase retardation. Center column: the corresponding on-axis intensity with (a) high frequency, high contrast sinusoidal modulation, (b) flat top self-imaging bottle beam distribution, and (c) electrocardiogram waveform of simulation (Sim) and experiment (Exp) results. Right columns: the corresponding generalized Bessel beams detected in experiment.

We have also demonstrated that the shape of the on-axis intensity profile can be an arbitrary shape defined digitally by users. We used a typical waveform acquired in electrocardiography to modulate the on-axis intensity. As seen in figure 6(c), the distinct features of P, Q, R, S, and T waves can be successfully encoded to a Bessel beam.

4. Discussion

'Generalized axicon' first mentioned in [21] was used to describe axicon-like lenses which could generate arbitrary on-axis intensity profiles. As we have seen in section 2.1, an azimuthally independent field can be generated by composition of different classical zeroth-order Bessel beams; from another point of view, the phases to generate each individual Bessel beam are also superimposed to form an ultimate, complex axicon-like phase mask—a generalized axicon phase. Thus, we call the corresponding quasi-Bessel beam 'the generalized Bessel beam'. Similar to the quasi-Bessel beam, although its center lobe preserves the beam diameter within a certain range, its side lobes present more complicated distribution patterns than those of the classical Bessel beam. The 3D distribution of flat top Bessel beam is shown in figure 7(a) as an example. The transverse intensity at $z = 6$ mm and $z = 10$ mm are shown in figures 7(b) and (c). The intensity profile at 6 mm is a composition of different Bessel functions while that of 10 mm is more like a Bessel function. The diameter of the central lobe is well maintained within the designed region, as shown in figure 7(c), which is similar to the so-called 'non-diffractive' property in the case of the quasi-Bessel beam. We believe the generalized Bessel beam also have self-reconstruction property if we see it as a bunch of co-propagating Bessel beams though further studies are needed. As central lobes of such beams are useful in most applications, the intensity distributions of side lobes are not of concern.

We have demonstrated above that the iterative optimization method is a powerful tool to shape the on-axis intensity profile of zeroth-order quasi-Bessel beams to virtually any given functions. This method can be also used to shape the intensity profile of side lobes of higher-order Bessel beams, which have zero fields on the axis. Here, we use the first-order Bessel beam and its first non-zero lobe as an example to describe the general concept. We first used the zeroth-order Bessel beam as a 'substrate' to find the phase mask for engineering the on-axis intensity profile to a given shape, and we then superimposed a vortex phase on the found phase mask to transform the Bessel beam to the first-order one. The design was fine-tuned according to the intensity measurement on the side lobe. As shown in figure 8, using

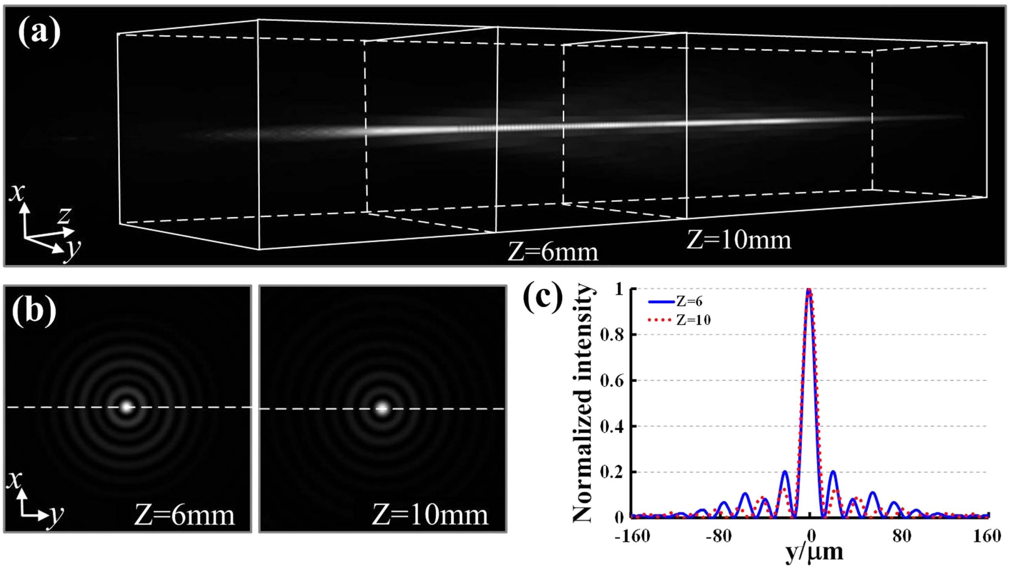

Figure 7. Simulation results of flat top Bessel beam. (a) 3D distribution of a flat top Bessel beam; (b) transverse intensity distribution at $z = 6$ mm and $z = 10$ mm; (c) intensity profile of dashed line in (b).

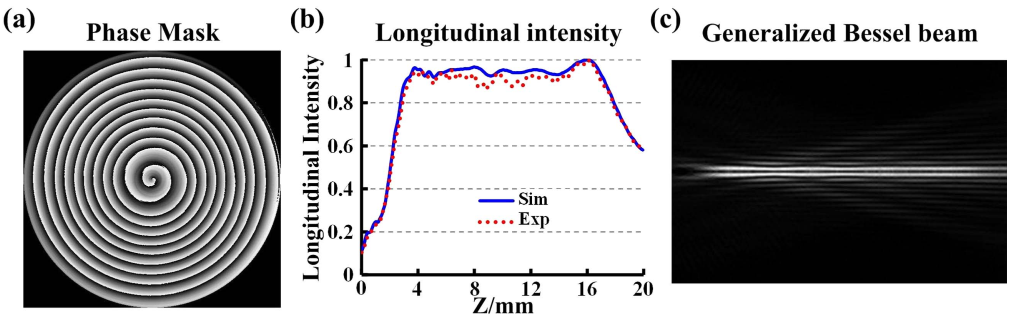

Figure 8. Simulation and experimental results of the flat top longitudinal intensity distribution of a first-order axicon phase. (a) Phase mask; (b) the corresponding on-axis intensity of (a); (c) distribution of generalized Bessel beam.

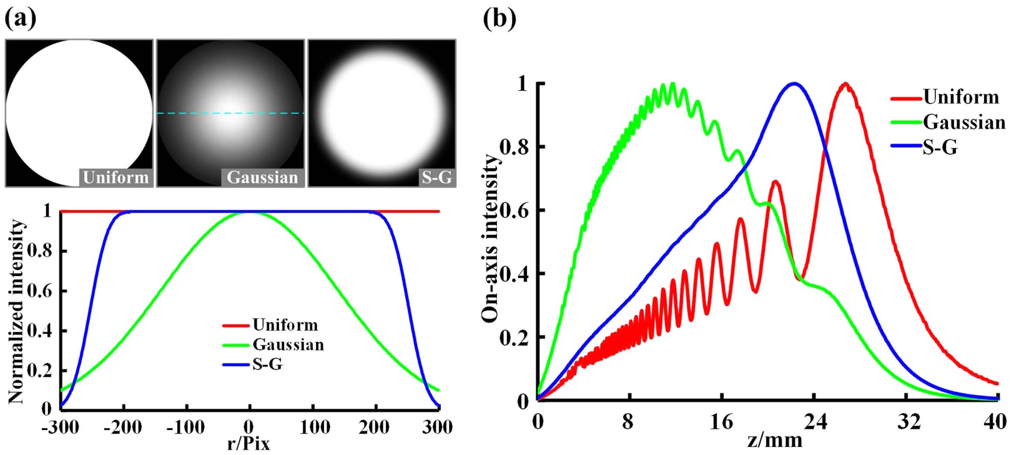

Figure 9. Simulation results of incident beams with different transverse intensity profiles and their corresponding intensity distributions along the propagation axis. (a) The apodization functions of circular aperture, Gaussian profile and super-Gaussian profile; (b) the corresponding on-axis intensity profiles. S-G represents super-Gaussian.

this strategy, we have successfully flattened the intensity profile of the side lobe of the first-order Bessel beam.

For simplicity of the design and implementation, we used plane waves with uniform intensity as incident beams. This is the reason we still see small oscillations in the profile. It is known that the transverse intensity distribution of the incident beam actually affects the on-axis intensity distribution [42]. To study this effect, we computed on-axis intensity profiles of

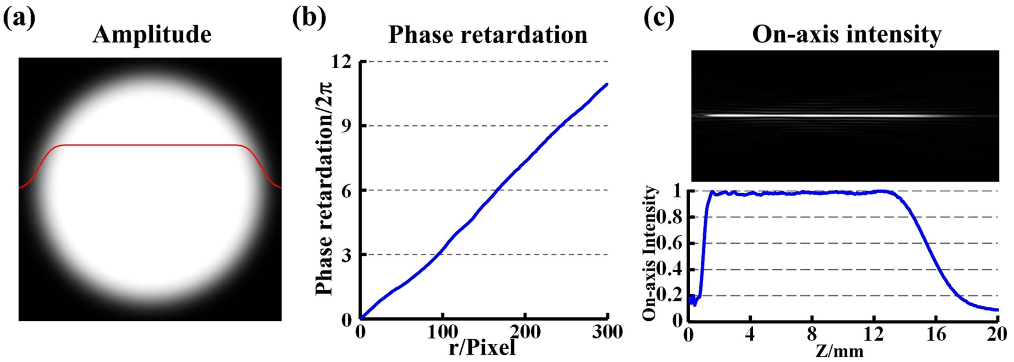

Figure 10. Simulation results of flat top design under super-Gaussian beam. (a) Amplitude of incident light; (b) the designed phase retardation; (c) the corresponding on-axis intensity profile.

Bessel beams generated by three functions: circular aperture, Gaussian, and super-Gaussian. The on-axis intensity of corresponding generated Bessel beams are shown in figure 9. By using Gaussian and super-Gaussian apodization, the edge effect can be suppressed, and thus the axial oscillations are reduced, but with the expense of shortened axial field length.

Then, we investigated if we could further flatten the on-axis intensity and reduce the oscillation by using our iterative method to optimize the phase mask design with a super-Gaussian incident beam. The optimized phase mask and the on-axis intensity are shown in figure 10. The oscillation is much smaller than that generated by plane waves (shown in figure 5(b)). Adding an intensity modulation on the top of the phase mask is certainly a good idea to yield an even higher quality on-axis intensity profile though an additional modulation device to control the amplitude is required in the experiment. It is an interesting idea that is worth investigating in the future study.

Finally, the design for partially coherent source and oblique illumination introduced in the thesis [27] were of interest in applications using Bessel beams. It might be worth further investigating the use of the GA iterative design process under those conditions.

5. Conclusion

Being able to accurately control the axial intensity of quasi-Bessel beams is of great interest in applications that either intend to use the unique properties of Bessel beams or require specific axial intensity profiles. Here we propose an iterative optimization based method to shape on-axis intensity profiles of quasi-Bessel beams arbitrarily. We have experimentally demonstrated that the proposed method can successfully generate zeroth-order Bessel beams with on-axis intensities customized to desired shapes. The same method is potentially applicable to shape the longitudinal intensity of higher-order Bessel beams. Our simulation studies have demonstrated that simultaneous optimization of the phase mask and the apodization function can reduce the intensity oscillation so that the quality of the on-axis intensity profile can be improved even further.

Acknowledgments

This research is supported by the Natural Science Foundation of China under Grant Nos. 61705256 and 11704405. TY is grateful for the support from National Institute of General Medical Sciences (R21GM-104683 and P20GM-103499) and a grant from the National Science Foundation (1539034).

ORCID iDs

Runze Li https://orcid.org/0000-0003-4506-8431

References

[1] Durnin J, Miceli J J and Eberly J 1987 Diffraction-free beams *Phys. Rev. Lett.* **58** 1499–501
[2] Durnin J 1987 Exact solutions for nondiffracting beams: I. The scalar theory *J. Opt. Soc. Am.* A **4** 641–51
[3] Garces-Chavez V, McGloin D, Melville H, Sibbett W and Dholakia K 2002 Simultaneous micromanipulation in multiple planes using a self-reconstructing light beam *Nature* **419** 145–7
[4] Ruffner D B and Grier D G 2012 Optical conveyors: a class of active tractor beams *Phys. Rev. Lett.* **109** 163903
[5] Lee K S and Rolland J P 2008 Bessel beam spectral-domain high-resolution optical coherence tomography with micro-optic axicon providing extended focusing range *Opt. Lett.* **33** 1696–8
[6] Yang Y, Lei M, Zheng J, Li R, Yan S, Yao B and Ye T 2013 Two-photon fluorescence stereomicroscopy with Bessel beams *Proc. SPIE* **8588** 85882K
[7] Yang Y, Yao B, Lei M, Dan D, Li R, Van M, Chen X, Li Y and Ye T 2016 Two-photon laser scanning stereomicroscopy for fast volumetric imaging *PLoS One* **11** e0168885
[8] Thériault G, Cottet M, Castonguay A, McCarthy N and Koninck Y D 2014 Extended two-photon microscopy in live samples with Bessel beams: steadier focus, faster volume scans, and simpler stereoscopic imaging *Front. Cell Neurosci.* **8** 139
[9] Song A, Charles A S, Koay S A, Gauthier J L, Thiberge S Y, Pillow J W and Tank D W 2017 Volumetric two-photon imaging of neurons using stereoscopy (vTwINS) *Nat. Methods* **14** 420–6
[10] Lu R *et al* 2017 Video-rate volumetric functional imaging of the brain at synaptic resolution *Nat. Neurosci.* **20** 620–8

[11] Fahrbach F O and Rohrbach A 2010 A line scanned light-sheet microscope with phase shaped self-reconstructing beams *Opt. Express* **18** 24229–44

[12] Planchon T A, Gao L, Milkie D E, Davidson M W, Galbraith J A, Galbraith C G and Betzig E 2011 Rapid three-dimensional isotropic imaging of living cells using Bessel beam plane illumination *Nat. Methods* **8** 417–23

[13] Zhao M, Zhang H, Li Y, Ashok A, Liang R, Zhou W and Peng L 2014 Cellular imaging of deep organ using two-photon Bessel light-sheet nonlinear structured illumination microscopy *Biomed. Opt. Express* **5** 1296–308

[14] Gao L, Shao L, Chen B C and Betzig E 2014 3D live fluorescence imaging of cellular dynamics using Bessel beam plane illumination microscopy *Nat. Protocols* **9** 1083–101

[15] Ahluwalia B P S, Yuan X C and Tao S H 2004 Generation of self-imaged optical bottle beams *Opt. Commun.* **238** 177–84

[16] Ahluwalia B P S, Yuan X C, Tao S H, Cheong W C, Zhang L S and Wang H 2006 Micromanipulation of high and low indices microparticles using a microfabricated double axicon *J. Appl. Phys.* **99** 113104

[17] Li L, Lee W M, Xie X, Krolikowski W, Rode A V and Zhou J 2014 Shaping self-imaging bottle beams with modified quasi-Bessel beams *Opt. Lett.* **39** 2278–81

[18] Golub I 2006 Fresnel axicon *Opt. Lett.* **12** 1890–2

[19] Burvall A 2004 Axicon imaging by scalar diffraction theory *PhD Dissertation* Microelectronics Information Technology IMIT

[20] Brzobohatý O, Čižmár T and Zemánek P 2008 High quality quasi-Bessel beam generated by round-tip axicon *Opt. Express* **16** 12688–700

[21] Sochacki J, Kołodziejczyk A, Jaroszewicz Z and Bara S 1992 Nonparaxial design of generalized axicons *Appl. Opt.* **31** 5326–30

[22] Bagini V, Frezza F, Santarsiero M, Schettini G and Spagnolo G S 1996 Generalized Bessel–Gauss beams *J. Mod. Opt.* **43** 1155–66

[23] Ornigotti M and Aiello A 2014 Generalized Bessel beams with two indices *Opt. Lett.* **39** 5618–21

[24] Fathallah A and Shalaby M 2011 Generalized Bessel beams in modified axially symmetric graded index structures *Appl. Opt.* **50** 3128–34

[25] Sochacki J, Staroński L R, Kołodziejczyk A and Jaroszewicz Z 1993 Annular-aperture logarithmic axicon *J. Opt. Soc. Am.* A **10** 1765–8

[26] Friberg A T 1996 Stationary-phase analysis of generalized axicons *J. Opt. Soc. Am.* A **13** 743–50

[27] Thaning A 2002 Asymptotic techniques in design and characterization of diffractive axicon *Thesis* Royal Institute of Technology

[28] Dong B, Yang G and Gu B 1996 Iterative optimization approach for designing an axicon with long focal depth and high transverse resolution *J. Opt. Soc. Am.* A **13** 97–103

[29] Zamboni-Rached M 2004 Stationary optical wave fields with arbitrary longitudinal shape by superposing equal frequency Bessel beams: frozen waves *Opt. Express* **12** 4001–6

[30] Zamboni-Rached M, Recami E and Hernández-Figueroa H E 2005 Theory of 'frozen waves': modeling the shape of stationary wave fields *J. Opt. Soc. Am.* A **22** 2465–75

[31] Vieira T A, Gesualdi M R R and Zamboni-Rached M 2012 Frozen waves: experimental generation *Opt. Lett.* **37** 2034

[32] Vieira T A, Zamboni-Rached M and Gesualdi M R R R 2014 Modeling the spatial shape of nondiffracting beams: experimental generation of frozen waves via holographic method *Opt. Commun.* **315** 374

[33] Dorrah A H, Zamboni-Rached M and Mojahedi M 2016 Generating attenuation-resistant frozen waves in absorbing fluid *Opt. Lett.* **41** 3702–5

[34] Čižmár T and Dholakia K 2009 Tunable Bessel light modes: engineering the axial propagation *Opt. Express* **17** 15558–70

[35] Ouadghiri-Idrissi I, Giust R, Froehly L, Jacquot M, Furfaro L, Dudley J M and Courvoisier F 2016 Arbitrary shaping of on-axis amplitude of femtosecond Bessel beams with a single phase-only spatial light modulator *Opt. Express* **24** 11495–504

[36] Holland J H 1975 *Adaptation in Natural and Artificial systems: An Introductory Analysis with Applications to Biology, Control, and Artificial Intelligence* (Ann Arbor, MI: University of Michigan Press)

[37] Goldberg D E 1989 *Genetic Algorithms in Search, Optimization and Machine Learning* (Reading, MA: Addison-Wesley)

[38] Haupt R L and Haupt S E 2004 *Practical Genetic Algorithms* (New York: Wiley)

[39] Li R *et al* 2017 Interleaved segment correction achieves higher improvement factors in using genetic algorithm to optimize light focusing through scattering media *J. Opt.* **19** 105602

[40] Zheng J, Yang Y, Lei M, Yao B, Gao P and Ye T 2012 Fluorescence volume imaging with an axicon: simulation study based on scalar diffraction method *Appl. Opt.* **51** 7236–45

[41] Device Operating Instructions PLUTO manual V1.2 (Holoeye PLUTO 2 NIR II)

[42] Jiang Z P, Lu Q S and Liu Z J 1995 Propagation of apertured Bessel beams *Appl. Opt.* **34** 7183–5